HYDROLOGICAL PROCESSES
Hydrol. Process. **23**, 858–873 (2009)
Published online 30 December 2008 in Wiley InterScience
(www.interscience.wiley.com) DOI: 10.1002/hyp.7211

Simulated soil water storage effects on streamflow generation in a mountainous snowmelt environment, Idaho, USA

M. S. Seyfried,[1]*,† L. E. Grant,[2] D. Marks,[1]† A. Winstral[1]† and J. McNamara[3]

[1] *USDA-Agricultural Research Service, Northwest Watershed Research Center, 800 Park Blvd, Plaza IV, Boise, ID 83712, USA*
[2] *University of California, Santa Barbara, CA 93106, USA*
[3] *Boise State University, Boise, ID 83725, USA*

Abstract:

Although soil processes affect the timing and amount of streamflow generated from snowmelt, they are often overlooked in estimations of snowmelt-generated streamflow in the western USA. The use of a soil water balance modelling approach to incorporate the effects of soil processes, in particular soil water storage, on the timing and amount of snowmelt generated streamflow, was investigated. The study was conducted in the Reynolds Mountain East (RME) watershed, a 38 ha, snowmelt-dominated watershed in southwest Idaho. Snowmelt or rainfall inputs to the soil were determined using a well established snow accumulation and melt model (*Isnobal*). The soil water balance model was first evaluated at a point scale, using periodic soil water content measurements made over two years at 14 sites. In general, the simulated soil water profiles were in agreement with measurements ($P < 0{\cdot}05$) as further indicated by high R^2 values (mostly $>0{\cdot}85$), y-intercept values near 0, slopes near 1 and low average differences between measured and modelled values. In addition, observed soil water dynamics were generally consistent with critical model assumptions. Spatially distributed simulations over the watershed for the same two years indicate that streamflow initiation and cessation are closely linked to the overall watershed soil water storage capacity, which acts as a threshold. When soil water storage was below the threshold, streamflow was insensitive to snowmelt inputs, but once the threshold was crossed, the streamflow response was very rapid. At these times there was a relatively high degree of spatial continuity of satiated soils within the watershed. Incorporation of soil water storage effects may improve estimation of the timing and amount of streamflow generated from mountainous watersheds dominated by snowmelt. Copyright © 2008 John Wiley & Sons, Ltd.

KEY WORDS streamflow; soil processes; snowmelt; mountain area; soil water balance modelling

Received 30 May 2008; Accepted 21 October 2008

INTRODUCTION

Streamflow generated from snowmelt in mountain river basins is the primary source of water for more than 60 million people in the western USA (Bales *et al*., 2006). As population-driven demands on water resources mount, and climatic trends persist (Barnett *et al*., 2008), it becomes increasingly critical that improved methods are developed for describing and predicting snowmelt-generated streamflow. One approach to accomplishing this improvement may involve a more explicit consideration of soil processes. While the critical role of soil in modifying and modulating streamflow generation during rainfall events has been exhaustively documented with field research (Bazemore *et al*., 1994; Anderson *et al*., 1997; Wilcox *et al*., 1997; Collins *et al*., 2000), analogous research during snowmelt is relatively rare. This is partly due to the large measurement and modelling demands associated with snowmelt inputs, partly due to the added challenge of conducting field research in winter, and partly due to fact that the basic processes of water retention and transmission through soils are the same whether the inputs are from rainfall or snowmelt. The result is that snowmelt–runoff models are either poorly supported with field data, or ignore soil processes entirely. However, conditions that are often associated with snowmelt are sufficiently different from rainfall to warrant specific attention.

One such condition is very high local spatial variability of snowmelt inputs to the soil (Winstral and Marks, 2002; Williams *et al*., in review). Topographic and vegetative features on the scale of tens of metres may cause large differences in the amount of snow accumulation, and hence the timing and amount of water input to the soil, in a manner very different from that in rainfall-dominated watersheds. For example, in snowmelt- dominated watersheds, the wettest soils may be found at or near the topographic high point in the watershed due to snow distribution (Seyfried and Wilcox, 1995; Flerchinger and Cooley, 2000), as opposed to topographic lows as is generally assumed in rainfall-dominated watersheds. In addition, snowmelt is strongly affected by solar exposure, and can therefore vary considerably over small distances in response to variations in topography or vegetative cover.

* Correspondence to: M. S. Seyfried, USDA-Agricultural Research Service, Northwest Watershed Research Center, 800 Park Blvd, Plaza IV, Boise, ID 83712, USA.
E-mail: mark.seyfried@ars.usda.gov
† The contribution of M.S. Seyfried, D. Marks and A. Winstral to this article was prepared as part of their official duties as a United States Federal Government employee.

Another condition differentiating snowmelt from rainfall is that melt water tends to enter wet soil with relatively high local groundwater conditions because snowmelt may be regarded, in some respects, as a single, protracted event. Snowmelt releases months of accumulated precipitation in a relatively short time. The rate of soil water input varies considerably during the snowmelt 'event', but because it occurs when evaporative demand is low, water loss from the soil is due primarily to drainage, and conditions remain very wet. Warm dry weather, which normally results in soil drying, accelerates snowmelt, resulting in even wetter conditions. In addition, basic energy balance constraints control the melt rate such that, while daily snowmelt water inputs may be quite high, melt water flux to soil is generally much less than the instantaneous precipitation fluxes associated with infiltration excess overland flow generation (e.g. during thunderstorms). Thus, input water tends to infiltrate into the soil and groundwater. Note that in this study we do not consider frozen soil effects on runoff because they are generally minimal under deep snow cover and forested ecosystems that are primarily responsible for water supply (Lindstrom *et al*., 2002; Whitaker and Sugiyama, 2005; Zhang, 2005; James and Roulet, 2007; Iwata *et al*., 2008).

This condition of high watershed 'wetness' during snowmelt inputs is critical in light of recent research demonstrating that watersheds often require specific, threshold levels of input (rainfall or snowmelt) to generate streamflow (Western *et al*., 2003; Buttle *et al*., 2004; Laudon *et al*., 2004; Tromp-van Meerveld and McDonnell, 2006). Once the threshold is exceeded, subsequent inputs translate very rapidly into streamflow. One explanation for this is that the threshold amount of input causes the watershed to become laterally 'connected', for example by a laterally continuous aquifer, and therefore capable of rapid transport of water from throughout the watershed to the channel (Western *et al*., 2003; Tromp-van Meerveld and McDonnell, 2006). This kind of very rapid streamflow response has been documented specifically for snowmelt (Flerchinger *et al*., 1992). Where operative, this has two important implications. First, once the streamflow generation input threshold has been exceeded, snowmelt dynamics and streamflow dynamics will be very tightly linked. Second, some of the year-to-year variations in streamflow generation from snowmelt will be linked to the amount of pre-snowmelt water input relative to the threshold.

It is clear in the previously cited research and other detailed field studies (Peters *et al*., 2003) that the threshold amount of input water is probably closely related to soil water status. This is consistent with a long history of rainfall–runoff studies linking streamflow initiation during rainfall to a soil water 'abstraction' amount (see Steenhuis *et al*., 1995 and Schneiderman *et al*., 2007 for recent examples). We have demonstrated a strong link between soil water content and streamflow dynamics during snowmelt in watersheds of contrasting geologies (granite and basalt) in south-west Idaho (Grant *et al*., 2004; McNamara *et al*., 2005). Similar observations by the Natural Resources Conservation Service, the agency responsible for snowmelt forecasting in much of the USA, have prompted the installation of soil water instrumentation at snow monitoring sites. In these cases, the link between soil water and streamflow is based on necessarily limited numbers of observations. In order to progress beyond these observations and use the soil water–snowmelt linkage to improve water management, a soil water model that can be extended beyond experimental watersheds is needed. Relatively simple, functional soil water balance models may be sufficient for the purpose. In this work we explore the use of this modelling approach in a snowmelt-driven watershed.

The conceptual basis for this approach is a one-dimensional, point-scale soil profile. Given the relative lack of model testing in a snowmelt environment, it is important to evaluate the use of a point-scale soil water balance model in that setting. A first objective was to determine if this modelling approach could effectively describe soil water dynamics in a snowmelt environment. This was done using field-measured soil water contents collected at multiple sites over two years. If this approach is to be useful for estimating streamflow generation thresholds, it must be applied to spatial domains, most effectively, watersheds. A second objective, was to spatially distribute the one-dimensional model across a watershed and determine how watershed-scale soil water is related to streamflow generation thresholds. Model-estimated soil storage was compared with measured streamflow generation in an instrumented watershed for this purpose.

METHODS

Field conditions

Site description. The study was conducted in the Reynolds Mountain East watershed (RME), located in the headwaters at the southern edge of the Reynolds Creek Experimental Watershed (RCEW) in south-west Idaho (Figure 1). The RCEW was established in 1960 by the Agricultural Research Service, US Department of Agriculture, and is located 80 km south-west of Boise, Idaho. Reynolds Creek is a perennial stream with a watershed area of 239 km^2, flowing north to the Snake River (Seyfried *et al*., 2001b). A comprehensive description of the RCEW and the data collected there can be found in a series of data reports (Marks, 2001).

The RME watershed encompasses a 0·38 km^2 portion of the Reynolds Creek headwater region with elevations ranging from 2020 m to 2140 m (Figure 1). Long-term (>30 years) average annual precipitation at RME is 866 mm and is concentrated in the winter months, with July and August typically very dry (Hanson *et al*., 2001). The long-term average annual streamflow, measured at a weir that defines the watershed, is 523 mm. With the exception of occasional rain-on-snow events, the greatest flows are nearly concurrent with springtime

DOI: 10.1002/hyp

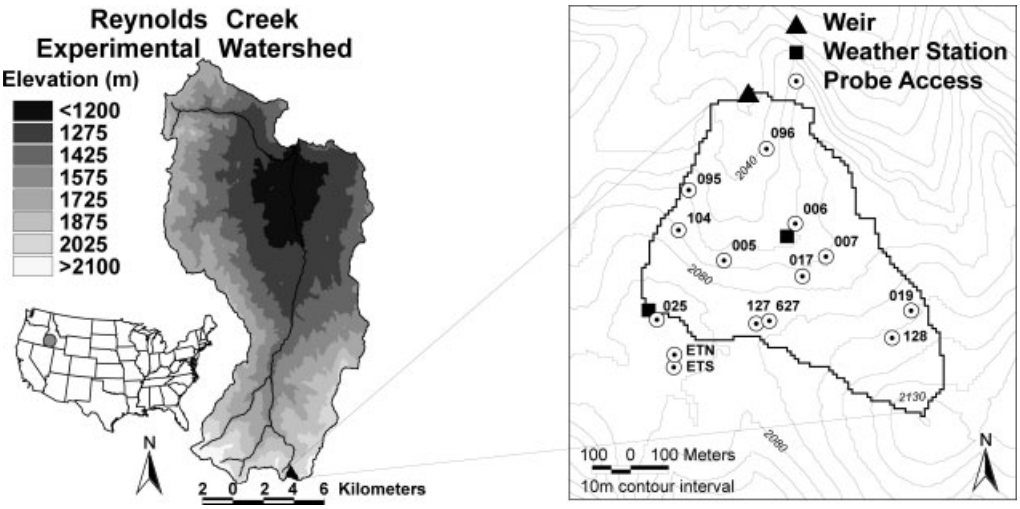

Figure 1. General map of the RCEW with locations within the RME of neutron probe access tubes, weather stations and the weir

maximum snowmelt, typically occurring in late April to early May (Pierson *et al*., 2001). Flow diminishes during the dry summer months to a very low discharge ($<0{\cdot}00014$ m^3 s^{-1}) that continues into fall and winter. The growing season average pan evaporation of 795 mm (Nayak *et al*., submitted) is much greater than the water potentially available for transpiration estimated from the difference between precipitation and streamflow (about 340 mm).

About 70% of the mean annual precipitation arrives at RME as snow (Hanson and Johnson, 1993), and the snowpack that develops is persistent throughout the winter and spatially continuous except on exposed ridges. In contrast to rain, which is evenly distributed across RME, the spatial distribution of snow is strongly affected by wind patterns, topography and vegetation and preferentially accumulates in drifts and wind-protected areas (Winstral and Marks, 2002). Thus, snow drifts, which cover about 9% of the RME surface, contribute 15–20% of the melt water input, and wind-protected areas contribute another 25% (Marks *et al*., 2002).

Soils in the RME were formed on slopes ranging from nearly level to 40% and have textures ranging from loam to clay with widely varying coarse fragment contents that generally increase with depth and proximity to bedrock. Soil depths range from extremely shallow (rock outcrops in places) to greater than 3 m. Parent material consists of shallow surficial loess deposits over basalt and latite.

Vegetation at the RME is dominated by mountain big sagebrush (*Artemesia tridentata vaseyana*), either in dense stands with snowberry (*Symphoricarpos oreophilus*) or sparse stands without snowberry. Rocky ridges have little or no vegetation surrounded by a sparse coverage of low sagebrush (*Artemesia arbuscula*) with mixed grasses and forbs. Dry meadows are dominated by grasses and forbs. Groves of quaking aspen (*Populus tremuloides*) are found either under or immediately downslope of snow drifts in upland areas, or associated with willows in riparian areas. There are also small areas of conifers, dominated by Douglas fir (*Pseudotsuga menziesii*) in protected, non-drift areas.

Meteorological streamflow data. The basic meteorological data, including solar radiation, incoming thermal radiation, air temperature, vapour pressure, wind speed, and soil temperature were measured by standard methods (Hanson *et al*., 2001) at two sites in RME (Figure 1). Wind-corrected precipitation was measured with a dual gauge, weighing bucket system at both sites as described by Hanson (2001). Streamflow was measured at a V notch weir as described in Pierson *et al*. (2001).

Soil water content. Soil water content (θ) data were collected by neutron probe for water years 2001 and 2003 (the period from 1 October to 30 September is conventionally defined as a water year in snowmelt-driven watersheds). Details of data collection and instrument calibration are described in Seyfried *et al*. (2001c) and Grant *et al*. (2004). Data were collected at 12 locations in the RME sub-basin during water year 2001 (WY2001). We expanded the measurement site network to 13 access tube sites in WY2003, 11 of which coincided with sites from WY2001. Tube locations are distributed throughout the catchment or immediately adjacent to it (Figure 1) and are intended to represent different landscape characteristics of soil, topography and vegetation (Table I). Two landscape types not represented are areas of little or no soil cover, due to the difficulty of inserting access tubes in rock, and areas under deep (>2 m) snow drifts, because the required extension tubes tend to be sheared by lateral, internal snow movement. The access tubes vary in depth from 55 cm to 330 cm, according to soil thickness. Many of the tubes were drilled into place and it was believed that they were installed in bedrock. Measurements were made at depths of 15 cm, 30 cm, and then at intervals of 30 cm, providing continuous θ information through the root zone to bedrock. Snow depth was also measured at each access tube site.

The neutron moderation method has a long history (Gardner and Kirkham, 1952) and the strengths and

DOI: 10.1002/hyp

Table I. Characteristics of neutron access tubes used in this analysis

Tube label	Elevation (m)	Tube depth (cm)	Clay content (%)	Coarse frag. content (%)	Vegetation type
095	2060	285	28	59	MS
096	2045	185	25	37	MSS
005	2069	358	20	57	C
006	2060	127	45	5	AW
007	2073	72	33	13	MS
017	2075	195	33	31	MSS
019	2103	135	31	31	LS
025	2099	100	17	40	MS
104	2069	88	20	60	MSS
127	2084	175	31	31	MSS
128	2118	81	30	15	MSS
ETN	2092	112	24	40	MS
ETS	2087	127	24	40	MS
627	2085	157	35	30	MSS

Vegetation types are: mountain sagebrush (MS), mountain sagebrush/snowberry (MSS), conifer (C), Aspen/willow riparian (AW) and low sagebrush (LS).

weaknesses are well documented (Hignett and Evett, 2002). Some advantages of the method are: (i) the measurement volume is almost two orders of magnitude greater than most electronic methods (a sphere approximately 15 cm in radius); (ii) site installation creates very little disturbance; (iii) addition of sites is relatively inexpensive; and (iv) the data are unaffected by soil freezing or temperature fluctuations in general. These assets make the method ideally suited to making extensive measurements of soil water storage. On the other hand, data are necessarily widely spaced 'snapshots' because the site must be visited to obtain data.

Simulation

Snowcover energy and mass balance. Most of the water entering the soil at RME is from snowmelt and cannot be measured directly as precipitation, but must be calculated from simulations of snow accumulation and melt. In this study, the *Isnobal* snow energy and mass balance model (Marks *et al*., 1999a), coupled with a wind field and snow redistribution model (Winstral and Marks, 2002), was used to simulate hourly snowcover development and melt for WY 2001 and WY 2003. Co-registered, 10×10 m grid digital elevation model and vegetation coverage maps were used as the basis for model simulations. *Isnobal* generates hourly output images of energy fluxes, mass fluxes and snow conditions. Marks *et al*. (1999b) presented a detailed description of the equations solved and a discussion of the structure of the model. One such output, the surface water input (SWI), which includes meltwater, rainwater that passes through the snowcover, and rain falling directly on the soil surface, was used as water input to the soil. The distributed meteorological variables required to drive the model are generated using data collected at the two meteorological stations at RME (Figure 1). The *Isnobal* model has been tested extensively at RME where it has been shown to predict accurately patterns of snow water equivalent and snow covered area, including wind scour and deposition (drifting) when coupled to a wind-field and snow redistribution model (Marks *et al*., 2002; Winstral and Marks, 2002; Winstral *et al*., 2008).

Soil water balance. Soil water content (θ) was simulated using a capacitance parameter based, functional soil water balance model (Addiscott, 1993). The resultant fluxes were calculated from θ differences. The model is described in detail in Seyfried (2003). Briefly, the soil is conceived as being composed of multiple layers, each with specified θ values that correspond to the plant extraction limit (θ_{PEL}), field capacity (θ_{FC}) and saturation (θ_{SAT}). Note that θ_{PEL} is analogous to permanent wilting point but, since most of the native vegetation does not wilt and the traditional 1·5 MPa soil water suction almost certainly does not apply (Pockman and Sperry, 2000), we use θ_{PEL} terminology. All water is assumed to flow vertically downward within the root zone, sequentially satiating each layer and draining to the next layer when θ is greater than θ_{FC}. Drainage proceeds as an exponential function of time as described by Hillel (1980). Throughflow (TF) is defined as the amount of water that flows out of the root zone. No TF occurs unless the bottom soil layer water content exceeds θ_{FC}. Transpiration is calculated using the Priestly–Taylor (1972) equation for potential evapotranspiration and modified by plant leaf area index (Rose, 1984; Seyfried, 2003) and by θ (Shuttleworth, 1993). Root distribution with depth is assumed to be as described by Jackson *et al*. (1996). For this application, values of θ_{PEL} and θ_{FC} were estimated from the neutron probe soil water dataset using moist but stable values for θ_{FC} and seasonal minimum values for θ_{PEL} as suggested by Ratliff *et al*. (1983) and Ladson *et al*. (2006) for accurate determination of those values.

This somewhat empirical approach to soil water modelling is widely used for agronomic crop modelling (Hanks, 1974; Ritchie, 1981) as well as various hydrology models (Evans *et al*., 1999). In the context of snowmelt modelling, it has the advantages that: (i) the linearity of functional soil parameters (e.g. θ_{PEL} and θ_{FC}) facilitates

DOI: 10.1002/hyp

transfer across scales; (ii) functional soil parameters are inherently less variable in space and can be estimated with greater accuracy from soil texture information than parameters such as hydraulic conductivity or the soil moisture characteristic; and (iii), the computational simplicity of functional models allows distributed modelling at relatively large scales with modest computer resources.

The fundamental disadvantage of the approach is that it does not calculate flow based on potential gradients that are known to govern soil matrix flow. This requires that four critical assumptions apply reasonably well within the root zone. The first is that there are identifiable values for θ_{FC} and θ_{PEL} that approximate a drainage limit and plant extraction limit. The second, is that all water that lands on the soil, from rain or snow, moves vertically into the soil. There is no way of calculating overland flow in the model. The third assumption is that, water entering the soil sequentially 'fills' each soil layer to the satiation point, θ_{FC}, prior to drainage. This assures that the soil storage capacity is exceeded before TF and streamflow generation. The fourth assumption is that there is no net lateral subsurface supply of water (i.e. net lateral flow to the channel occurs below the root zone). Additional model assumptions (e.g. related to transpiration), which are not critical to water storage and streamflow generation during snowmelt in this basin, are described elsewhere (Seyfried, 2003).

Spatial distribution. Given the assumptions discussed above, watershed soil water storage can be modelled as an assemblage of independent cells with various combinations of SWI, soil and vegetation properties, provided the spatial resolution of the cells is sufficient to capture critical deterministic variability. The 10 m square grid used appears to be sufficient, at least for snowmelt dynamics (Marks *et al.*, 2002). Each 10 m cell was parameterized with one of eight vegetation/soil types which were identified using a classified image (Figure 2) as described by Grant (2005). Corresponding soil parameter values (e.g. θ_{FC}) for six of the eight categories were determined from the point-scale modelling described above (Table II). Since we have no measured data for bare ground or soils under snow drifts, a combination of a detailed soil survey made of RME and soil water data collected at a similar site with time domain reflectometry about 3 km from RME in the RCEW, was used.

RESULTS

Profile simulations

Overview. An overview of the results obtained from the profile simulations is illustrated in Figures 3 and 4, where the translation of atmospheric inputs to SWI (using *Isnobal*), is linked to the progressive water storage in the soil profile and fluxes to TF and/or transpiration and evaporation. Two sites were selected (096 for WY2001 and 127 for WY2003) to provide some idea of the differences among sites.

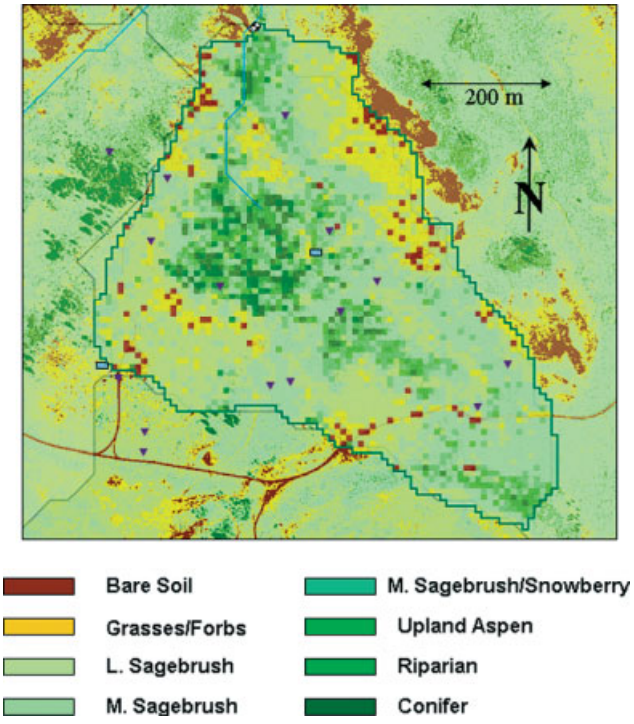

Figure 2. Vegetation/soil cover types based on an aerial photograph

The WY2001 results (Figure 3) show that precipitation inputs were more or less evenly distributed from 1 October to mid-June, after which the typical very dry summer commenced (Figure 3a). Soil water inputs, however, are heavily weighted toward two 10 day snowmelt events, in late March and late April, that define the snowmelt season at that site (Figure 3b). This exemplifies the temporal disconnection between precipitation and SWI described previously.

Simulated soil layers in Figure 3c are centred on the neutron probe measurement depths to facilitate comparison. The simulated transfer of water through the profile starts with dry soil (assumed to be θ_{PEL} on 1 October except the upper 5 cm, which are 0·02 m^3 m^{-3} due to direct soil evaporation). Water content increases with SWI and water moves downward after θ_{FC} for a given layer is exceeded.

The total water stored in the root zone (S, mm) is illustrated in Figure 3d. Storage, from either measurements (points) or simulation (line) is calculated as

$$S = \sum_{i=1}^{i=numlayer} \theta_i T_i \qquad (1)$$

where T is the soil layer thickness, i is the soil layer and *numlayer* is the number of soil layers in a given soil profile. Note that, for a 150 cm deep profile, storage is actually calculated to a depth of 165 cm due to the 15 cm neutron probe measurement radius. This procedure has been shown to provide accurate measurement of changes in soil water storage measured with a lysimeter (Seyfried *et al.*, 2001a).

The profile soil water storage capacity S_{FC}, is analogous in concept to θ_{FC} for a given soil layer and is

DOI: 10.1002/hyp

Table II. Soil parameter values used in WY2001 and WY2003 simulations

Soil/Veg Class	Layer	Depth (cm)	θ_{SAT}	θ_{FC}	θ_{PEL}	$S_{FC} - S_{PEL(\mathrm{mm})}$	Area (%)
	1	0–5	0·170	0·100	0·030	69	2·7
Bare	2	5–22·5	0·110	0·070	0·030		
Soil	3·	22·5–45	0·060	0·040	0·020		
	4	45–75	0·380	0·200	0·020		
	1	0–5	0·498	0·299	0·100	200	8·6
Mountain	2	5–22·5	0·498	0·299	0·100		
Sagebrush/	3	22·5–45	0·491	0·305	0·119		
Snowberry	4	45–75	0·436	0·291	0·147		
	5	75–105	0·448	0·323	0·197		
	6	105–135	0·400	0·292	0·183		
	7	135–165	0·387	0·288	0·190		
	1	0–5	0·435	0·270	0·105	131	10·74
Grass/	2	5–22·5	0·435	0·270	0·105		
Forbs	3	22·5–45	0·560	0·375	0·190		
	4	45–75	0·540	0·365	0·190		
	1	0–5	0·493	0·277	0·060	253	1
	2	5–22·5	0·493	0·277	0·060		
	3	22·5–45	0·352	0·217	0·081		
Upland	4	45–75	0·327	0·212	0·097		
Aspen	5	75–105	0·314	0·207	0·099		
	6	105–135	0·283	0·188	0·092		
	7	135–165	0·303	0·205	0·107		
	8	165–195	0·232	0·155	0·078		
	9	195–225	0·246	0·160	0·074		
	1	0–5	0·490	0·320	0·150	96	30·9
Low	2	5–22·5	0·490	0·320	0·150		
Sagebrush	3	22·5–45	0·470	0·320	0·170		
	4	45–75	0·280	0·200	0·120		
	1	0–5	0·400	0·295	0·075	302	8·7
Riparian	2	5–22·5	0·400	0·295	0·095		
	3	22·5–45	0·400	0·310	0·140		
	4	45–75	0·550	0·475	0·260		
	5	75–105	0·470	0·400	0·250		
	6	105–135	0·480	0·440	0·300		
	1	0–5	0·434	0·020	0·267	162	35·2
	2	5–22·5	0·434	0·020	0·267		
Mountain	3	22·5–45	0·399	0·103	0·251		
Sagebrush	4	45–75	0·338	0·118	0·228		
	5	75–105	0·392	0·138	0·265		
	6	105–135	0·323	0·187	0·255		
	1	0–5	0·493	0·277	0·060	253	2·3
	2	5–22·5	0·493	0·277	0·060		
	3	22·5–45	0·352	0·217	0·081		
Conifer	4	45–75	0·327	0·212	0·097		
	5	75–105	0·314	0·207	0·099		
	6	105–135	0·283	0·188	0·092		
	7	135–165	0·303	0·205	0·107		
	8	165–195	0·232	0·155	0·078		
	9	195–225	0·246	0·160	0·074		

represented, at tube 096, by the horizontal bar at 475 mm and is calculated as

$$S_{FC} = \sum_{i=1}^{i=numlayer} \theta_{FCi} T_i. \qquad (2)$$

To continue the field capacity analogy, TF occurs only when $S > S_{FC}$. Although there are unusual circumstances where this is not strictly the case, it's reasonable to regard S_{FC} as the TF threshold.

Profile S data (points) and simulation (line) values in Figure 3d are in close agreement over the year, indicating good simulation of the overall profile water balance. After starting under very dry conditions ($S = 263$ mm), the threshold S_{FC} value was exceeded when the first major snowmelt event in late March satiated the profile and generated TF. Subsequent SWI, which occurred with $S \geq S_{FC}$, resulted in three somewhat distinct TF events. The first two were in response to snowmelt, the third due to the relatively large rainfall in mid-May. After that rainfall, the snow cover was gone, there was a rapid

DOI: 10.1002/hyp

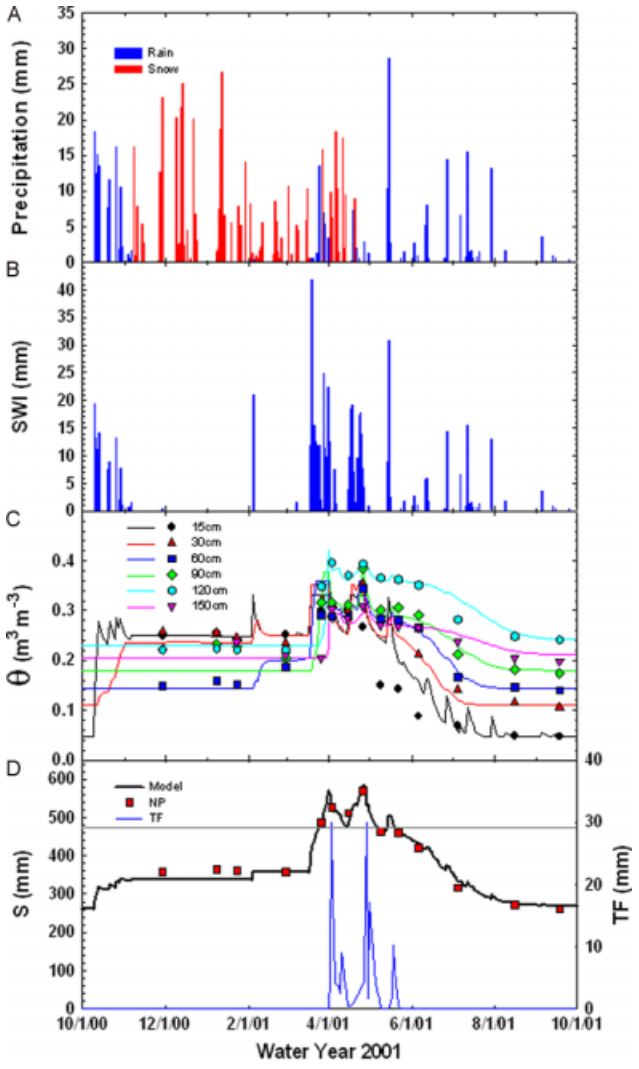

Figure 3. Profile soil water dynamics at site 096 for WY2001. (A) Precipitation partitioned between rain and snow, measured at the gauge near the centre of the watershed (Figure 1). (B) *Isnobal* calculated SWI. (C) Simulated (continuous line) and measured (symbol) θ. (D) Simulated (line) and measured (symbol) profile water storage, profile storage capacity (horizontal line) and throughflow (horizontal line)

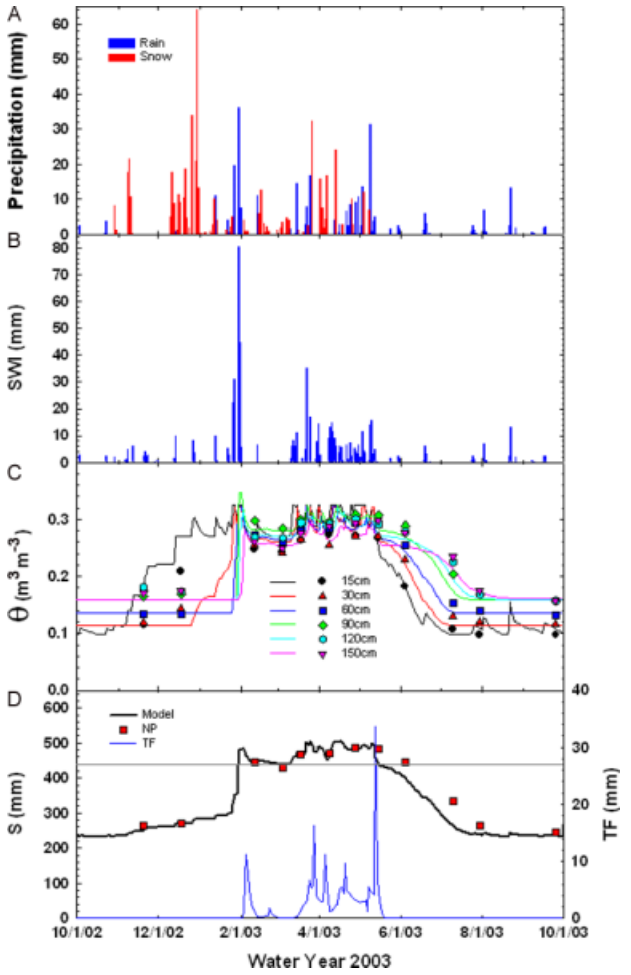

Figure 4. Profile soil water dynamics at site 127 for WY2003. (A) Precipitation partitioned between rain and snow, measured at the gauge near the centre of the watershed (Figure 1). (B) *Isnobal* calculated SWI. (C) Simulated (continuous line) and measured (symbol) θ. (D) Simulated (line) and measured (symbol) profile water storage, profile storage capacity (horizontal line) and throughflow (horizontal line)

spring 'green up', and evapotranspiration rapidly dried the soil. Subsequent rainfall did not generate TF because it had little effect on S, with only the surface layers affected.

The weather in WY2003 was substantially different from WY2001 resulting in different θ, S and TF dynamics (Figure 4). At the end of January 2003 there was a moderately large winter rainfall (Figure 4a) that, combined with snowmelt, resulted in a much larger SWI event (Figure 4b). The input was sufficiently large that all soil layers to a depth of 150 cm were satiated (Figure 4c), resulting in TF generation (Figure 4d). This coincided closely with S exceeding S_{FC} (440 mm). Storage remained greater than or equal to S_{FC} for about $3\frac{1}{2}$ months, during which time small SWI events were rapidly translated into TF. As in 2001, the soil rapidly dried after a last mid-May rainfall, and subsequent rains had little impact on S or TF generation.

Statistics. Figures 3 and 4 present two 'typical' profile-years of simulation and data comparison. We analysed a total of 26 profile-years using linear regression statistics (simulated versus measured S or θ) and the absolute value of the average difference between the measured and simulated value (AD). These data are presented for each θ measurement depth as well as the calculated S for readings to 60, 90 and 120 cm in Table III.

The number of readings is about the same for both years and declines with depth due to the dominant relatively shallow soils. There is little trend in the θ accuracy either between the two years or with depth. Average difference values were between 0·015 m^3 m^{-3} and 0·003 m^3 m^{-3} for all the depths in both years. R^2 values for θ were reasonably high, generally between 0·85 and 0·95 with the notable exceptions of the 150, 180 and 210 cm data in WY2001. One of the major differences between the two years at those depths is a relatively narrow range of values in WY2001. Excepting the 150, 180 and 210 cm data in WY2001, slopes were close to 1 and y-intercept values were close to 0, indicating a lack of bias (Mulla and Addiscott, 1999).

DOI: 10.1002/hyp

Table III. Average difference between simulated and measured θ and S, linear regression statistics, and the number of samples for WY2001 and WY2003

	Depth cm	WY 2001					WY 2003				
		AD	R^2	y int	slope	N	AD	R^2	y int	slope	N
	15	0·023	0·875	0·026	0·982	159	0·031	0·8	0·024	0·945	166
	30	0·020	0·851	0·024	0·89	159	0·023	0·844	0·008	0·926	166
	60	0·016	0·893	−0·008	1·051	159	0·027	0·862	0·008	0·956	166
θ m^3 m^{-3}	90	0·014	0·905	0·003	0·986	131	0·017	0·922	0·012	0·957	128
	120	0·021	0·832	0·016	0·957	101	0·015	0·944	0·004	0·979	102
	150	0·024	0·622	0·083	0·584	53	0·016	0·893	0·011	1·02	63
	180	0·029	0·522	−0·027	1·483	26	0·023	0·845	0·034	1·03	26
	210	0·027	0·425	−0·006	1·333	26	0·024	0·855	0·03	1·091	26
	60	1·077	0·94	−0·018	1·045	159	1·385	0·901	0·649	0·963	162
S cm	90	1·141	0·949	0·089	1·03	131	1·616	0·918	0·886	0·973	128
	120	1·406	0·952	0·402	1·023	101	2·044	0·927	1·26	0·967	102

The AD values for S increased slightly (3 to 6 mm) with profile thickness both years, but when considered relative to the increase in total storage, agreement improved slightly with depth. Regression statistics for both years showed little trend with profile thickness and slopes are near 1, constants near 0 and R^2 values above 0·9. Almost all S statistics were slightly better in WY2001 than in WY2003. In general, the S statistics were somewhat better than the θ statistics when considered relative to the range of values encountered. This is a reflection of the fact that estimation of θ at a particular layer is a more rigorous test than S for the profile. For example, if a wetting front progressed 45 cm into the soil, but the model calculated a wetting depth of 60 cm, a large error in θ will result, but the S calculation under that scenario may be quite accurate. The accuracy of S simulation is more critical for the overall water balance objective because that is what affects TF and, ultimately, streamflow.

The good general agreement between modelled and measured values at least partly stems from the fact that critical parameter values (θ_{FC} and θ_{PEL}) were derived from the same data the model was evaluated with (Ratliff *et al*., 1983; Western and Grayson, 2000). The issue of parameterization is critical for the practical application of this modelling approach. We do not address that issue in this paper, but rather we take the good agreement between measured and simulated values to indicate that, the point-scale model provides an accurate accounting of soil water balance and therefore is a good means of evaluating S as a parameter related to streamflow generation. It is understood that if the basic assumptions behind the model are not appropriate for the conditions, or that the parameter values used are not reasonable, then the good agreement carries no such implication.

Assumptions. Here we examine the data and field observations to determine if they are consistent with the four assumptions critical to this model application listed in a previous section. The first assumption is that two constants can be identified that correspond to drainage cessation (θ_{FC}) and transpiration cessation (θ_{PEL}) such that the difference $\theta_{FC} - \theta_{PEL}$ defines the available or dynamic soil water. The use of θ_{FC} as a soil constant describing soil water movement is somewhat controversial, partly due to the way it has been misapplied in the past (see Hillel, 1980 for discussion). We found that soil water dynamics were invariably consistent with the existence of θ_{FC} in the sense that winter time θ values maintained consistent, similar high values. However, careful examination indicates that the 'effective' θ_{FC} was often lower during infiltration than during drainage. For example, the 30 cm θ at the ETS site was effectively at field capacity in early November of 2000 because θ at 60 cm, the next layer, increased (Figure 5). This would indicate that θ_{FC} is about 0·20 m^3 m^{-3}. However, during the drainage events in spring it would appear to be more like 0·24 m^3 m^{-3}. We believe that this does not invalidate the approach, but it clearly introduces some error in the estimation of S.

The primary evidence for the validity of θ_{PEL} is that each year the θ at all depths is quite stable during the very high evaporative demand, low precipitation months of August and September and tends to return to the same value each year. This is evident in all the data presented, except that the surface layers were usually wetted by

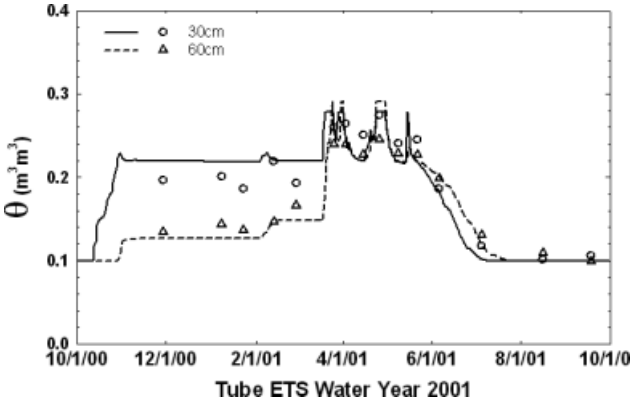

Figure 5. Measured and simulated soil water content at the ETS site for WY2001. The effective field capacity appears to be greater during drainage (about 0·20 m^3 m^{-3}), than during infiltration (about 0·24 m^3 m^{-3})

DOI: 10.1002/hyp

fall precipitation prior to the first measurement. The same, drought-tolerant vegetation remains as a constant during the study. With the exception of one site, which is discussed in detail shortly (006), all of the root zone parameter values used are within the range of values established for θ_{FC} and θ_{PEL} given high coarse fragment contents (Or and Wraith, 2002; Saxton and Rawls, 2006).

There are three lines of evidence that support the second critical assumption—that there is no overland flow. First, we have not observed overland flow despite considerable field time at the site. Admittedly, overland flow may take place under the snow cover and go undetected, but it has not been noted when the cover is patchy (a common condition). Second, the sediment load at the weir is very low. And third, the water balance generally agrees closely. That is, the water that *Isnobal* calculates as melt water, agrees closely with that measured with the neutron probe as a change in S. This is the case even though there are substantial differences in the quantity of input water across the watershed.

The third assumption, concerning the orderly progression of infiltration and wetting of the soil profile to θ_{FC}, is critical because it is the basis for estimating when the soil profile is 'satiated'. This kind of 'orderly' progression has been well documented for infiltration into dry soil similar to that experienced at Reynolds Mountain each summer (Wierenga *et al*., 1991). Consistent with this, we observed in all profiles for both years, a progressive wetting of the soil from the top to the bottom. The temporal separation of measurements is admittedly large, so that the wetting front progression was not always well documented. We note, however, that the progression is well documented very deep in the profile. At site 005, for example, a sequential wetting is evident to a depth of 300 cm (Figure 6). Hourly data collected at similar sites invariably show a vertical progression of wetting (McNamara *et al*., 2005).

Note that this assumption does not exclude macropore flow or bypassing. The only condition is that such flow occurs only when $\theta > \theta_{FC}$. In fact, it is likely that macropore flow occurs often during the snowmelt season. Note that simulated drainage from the soil profile often seemed to lag behind the actual value, due mostly to computational issues involved in the daily time step. This implies that water moved through a 150 cm soil profile within 1 day, which is indicative of bypassing, especially in heavy textured soils (Or and Wraith, 2002; Saxton and Rawls, 2006).

Among the data collected, all sites appear to be consistent with the first three assumptions. That is not true of the fourth assumption; that there is no net lateral subsurface flow in the root zone. At one site, 006 (Figure 7), this assumption appears to be violated. While θ values at 15 cm and 30 cm are similar to those at the other sites, the maximum (0·48 m^3 m^{-3}) and minimum (0·26 m^3 m^{-3}) values measured at 60 cm are greater than at any other site. The deeper layers, at 90 cm and 120 cm behave similarly and in a manner that is not consistent with draining to θ_{FC} or experiencing plant extraction to θ_{PEL}. The apparent θ_{PEL} (i.e. minimum) values of 0·40 m^3 m^{-3} and 0·44 m^3 m^{-3} are much greater than measured elsewhere, even for high clay content soils. These data indicate that a water table is maintained at sufficient proximity to the 120 cm measurement depth to maintain a very high water content year round (and for both years). Other evidence for this is: (i) there is relatively little change in S during the year, less than that for sagebrush, even though the site is covered by a stand of aspen that would certainly use more water than sagebrush; (ii) examination of the soil in the area near 006 yields observations of mottling and gleying indicative of reducing conditions and a high water table; and (iii) the position of the site near and topographically below two major snow drifts, near perennial springs and the point of initial channel formation.

This finding was not unexpected in that there must be some locations where lateral subsurface flow intersects the channel. In order to estimate the impact of this violation of assumptions, we ran the model as if there was a fixed water table depth below the root zone causing a capillary fringe into the root zone (120 and 90 cm) following work by Seyfried and Rao (1991). This results in an elevated 'effective' θ_{FC} that increases with proximity to the water table. It turns out that this change had little impact on the amount of TF calculated and

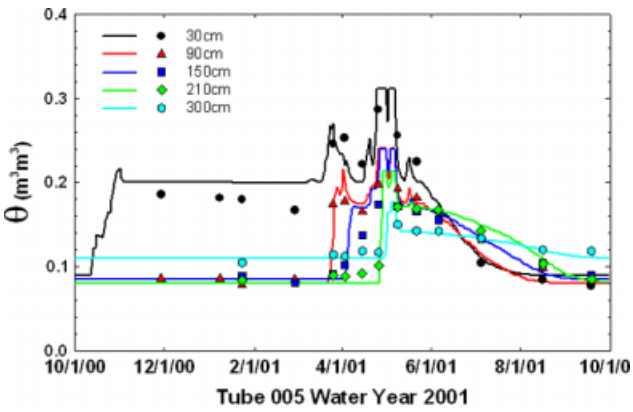

Figure 6. Measured and simulated soil water content for five depths at site 005, WY2001, the deepest tube monitored. We only present about half the layers to avoid cluttering the figure

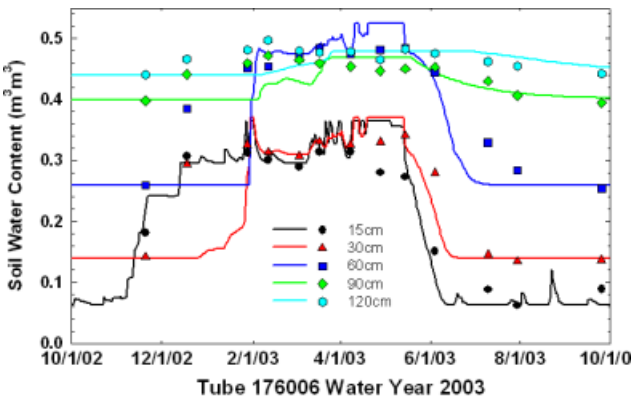

Figure 7. Measured and simulated soil water content for five depths at site 006, WY2003

DOI: 10.1002/hyp

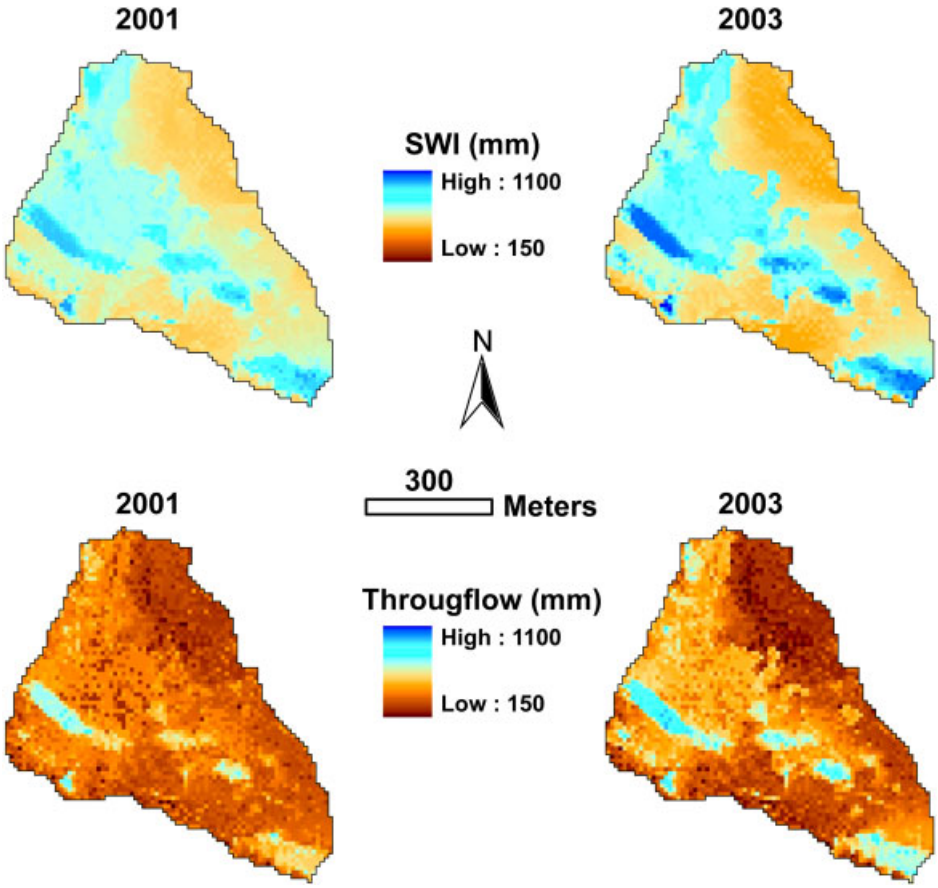

Figure 8. Spatial distribution of total SWI for WY2001 and WY2003 in mm and the spatial distribution of total TF for WY2001 and WY2003. Data are presented on the same scale to facilitate comparisons

had a very large effect on the amount of transpiration calculated. The calculated transpiration increased because the vegetation is effectively sub-irrigated during the dry summer months. Thus, while the assumption of no net lateral flow in the root zone is critical for the overall water balance calculation, it not is critical for TF calculations.

Distributed modelling

Spatial variability. We mentioned at the outset that a high degree of relatively small-scale spatial variability is a common characteristic of mountainous, snowmelt-driven watersheds. We illustrate this with Figure 8, which shows greater than twofold change in SWI in the space of one or two simulation cells (10 or 20 m). Winter snow distributions are even more dramatic due to the 'smoothing' effect that rainfall, which is uniformly distributed at this scale, has on the SWI distribution. The spatial SWI distribution patterns are similar for both years as consistent winds scour and deposit snow in similar locations each year. The two largest snow drifts and hence SWI inputs, are located at the extreme south-east corner of the watershed and near the western border. Total precipitation for WY2001 (740 mm) was slightly less than that in WY2003 (805 mm), and was more concentrated in the drifts in WY2003.

The range in TF is much greater than SWI due to the interactions between snow, soil and vegetation (Figure 8). For example, soils under the western drift are shallow and rocky with very sparse vegetation, so that annual TF was about 90 mm less than the annual SWI (i.e. there is relatively little storage or transpiration). Soils under the south-eastern drift are deeper and covered with aspen (enhancing transpiration) so that, whereas annual SWI is similar for the two drifts, annual TF is about 250 mm lower under the south-east drift. Some low annual TF sites have coniferous vegetation (Figure 2), deep soils and moderate snow accumulation (e.g. site 005, Figure 6). Most of the SWI at those sites is returned to the atmosphere due to a combination of high LAI and high S_{FC}. Other low annual TF sites are in scour zones that accumulate and melt very little snow.

Watershed storage. To evaluate the watershed-scale results, we introduce additional terms that are analogous to the profile capacitance terms described earlier. Thus, the watershed surface water input, SWI_W, watershed root zone water storage, S_W, watershed root zone storage capacity, $S_{FC,W,}$ and watershed throughflow, TF_W, are the spatial average value of the respective parameter for all cells for a given time step (usually one day). These terms are analogous to the equivalent depth of water in the watershed. If all soil layers are at field capacity, the storage at each cell will be the S_{FC} value, and S_W will equal $S_{FC,W,}$. In that case, the watershed is completely satiated and any additional water will cause TF.

DOI: 10.1002/hyp

This condition is highly unusual due to the variable inputs, and soil and vegetation properties within RME. In the following analysis, we use $S_{FC,W}$ as an index of a watershed-scale threshold storage that, when exceeded, results in streamflow.

In WY2001, the fall and early winter SWI_W resulted in increased S_W, but had no appreciable effect on streamflow (Figure 9). This changed during the first snowmelt event in late March when S_W increased abruptly, exceeding $S_{FC,W}$ (149 mm). The timing of measured streamflow initiation and modelled TF_W were practically identical, and S_W exceeded $S_{FC,W}$ shortly afterwards. During the first two weeks of April, SWI_W was very low allowing soils to drain to $S_{FC,W}$ and TF_W and streamflow to approach 0. Both streamflow and TF_W responded rapidly to the next snowmelt event in late April. The timing of TF_W spikes was similar to the streamflow spikes, although their magnitude was quite different. It is notable that the streamflow response to the large rainfall on 15 May occurred within the same day as the rainfall, while the corresponding TF_W spike was 2 days later. The volume of the response was similar for both even though the rainfall input was distributed evenly across the watershed. With the mid-May disappearance of snow cover and increase in evaporative demand, S_W quickly decreased below $S_{FC,W}$, TF_W went to 0 and streamflow, lagging somewhat behind TF_W declined to very low, pre-winter levels. There were 221 mm of streamflow during the time 'window' that S_W was above or near $S_{FC,W}$. If the two weeks following that period are included (accounting for the lagged streamflow decline), that number rises to 252 mm or 84% of the total annual streamflow.

Although the timing of events generating streamflow was quite different in WY2003, $S_{FC,W}$ acted as a threshold for both TF_W and streamflow as it had the prior year. As in WY2001, early season SWI_W events caused an increase in S_W, but had no effect on streamflow until S_W exceeded $S_{FC,W}$, in this case on 30 January, almost two months earlier than in WY2001. This resulted in initiation of both TF_W and streamflow both years. The S_W remained near $S_{FC,W}$ during the ensuing drop in SWI_W, and both streamflow and TF_W were highly responsive to inputs. The timing and amount of TF_W was generally much closer to that of streamflow in WY2003, being very rapid in both cases as S_W remained above $S_{FC,W}$ and highly responsive for the remainder of the season. Peak streamflow and TF_W occurred on 15 May, and both declined rapidly in spite of subsequent rainfall as watershed soils warmed and vegetation began to transpire. In WY2003, 336 mm, or 84% of the annual total streamflow exited the watershed during the window that S_W exceeded $S_{FC,W}$. If the two weeks at the end of the season are added for consideration, 372 mm or 93% of the annual total exited the watershed during that period.

Spatial distribution. One explanation for the very rapid streamflow response we observed is that points generating TF become connected with each other and the channel such that saturated, high permeability conduits can conduct water, unobstructed, from upland sources to the channel. This adds a spatial component to ideas conveyed in Figures 9 and 10 and implies that connectivity accompanies S_W values exceeding $S_{FC,W}$. To illustrate watershed connectedness we introduce one final storage variable, the normalized profile storage, S_N, which is defined as

$$S_N = \frac{S - S_{PEL}}{S_{FC} - S_{PEL}}. \tag{3}$$

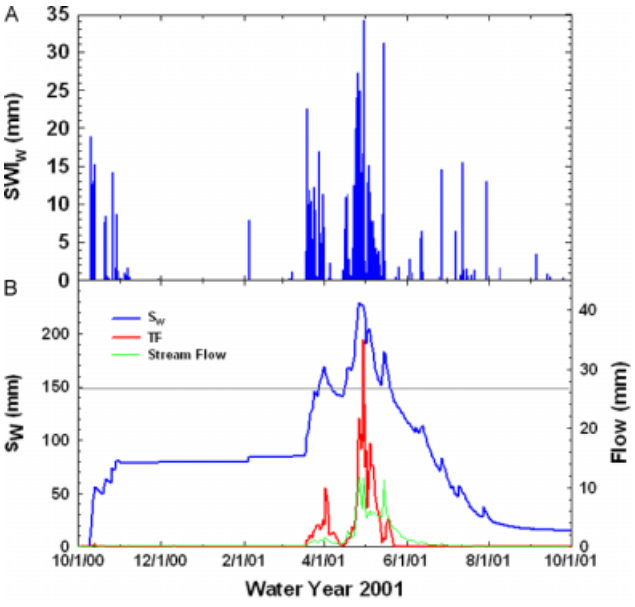

Figure 9. SWI_W, S_W, TF_W, and streamflow for WY2001. The horizontal line represents $S_{FC,W}$. Vertical lines indicate the dates illustrated spatially in Figure 11

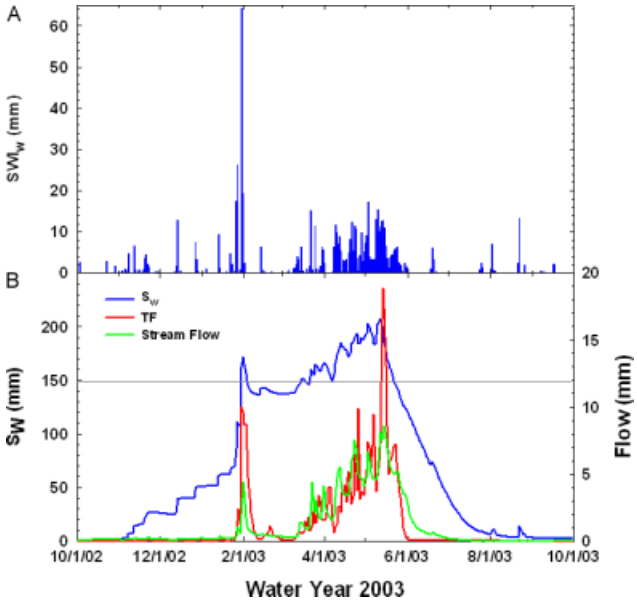

Figure 10. SWI_W, S_W, TF_W and streamflow for WY2003. The horizontal line represents $S_{FC,W}$. Both TF and streamflow are closely associated with time that S_W exceeds $S_{FC,W}$. Vertical lines indicate the dates illustrated spatially in Figure 12

DOI: 10.1002/hyp

S_N values of 1 or greater indicate that the soil profile is satiated and the profile is therefore highly responsive to inputs. We envision that interconnectedness may be expressed as a high density of cells with S_N close to or greater than 1.

We provide maps of the spatial distribution of S_N in temporal 'snapshots' to illustrate the linkage between the spatial distribution of soil water and the overall average watershed fluxes. On 6 Jan 01, S_W was about half $S_{FC,W}$ and S_N throughout the watershed was less than one (Figure 11). This picture remained unchanged until large inputs started on 18 March (Figure 9). By 20 March, after 35 mm of SWI, the situation was quite different, but S_N values in for the cells with deep soil in the centre of the watershed were considerably less than one and streamflow (Figure 9) had barely changed. By 1 April, the S_N values for almost all cells in the watershed (excepting the south-east drift), exceeded 1 and hence were potentially connected. Both TF and streamflow had risen substantially. On 27 April, in the midst of the second phase of snowmelt, S_N exceeded 1 for virtually all cells in the watershed, and streamflow was very sensitive to SWI_W (Figure 9). This condition persisted as the snow cover diminished but cell S_N values remained near 1 due to a lack of evaporation and transpiration. The watershed remained well connected until after a large rainfall event on 15 May. By 27 May, very little of the watershed was satiated and subsequent precipitation events had practically no effect on streamflow.

In WY 2003 (Figure 12), early season dry soils had received some water input by 7 January (Figure 10), but cells with $S_N < 1$ dominated the watershed and streamflow was unaffected by SWI_W. In the last 6 days of January the SWI_W exceeded 179 mm during a rain-on-snow event that caused a minor streamflow response while most of the watershed cells became satiated. Parts of the watershed, especially the south-eastern drift area, were still not contributing as S_N was less than 1. On 28 February, during a period of no SWI, the watershed was similar to 1 February with respect to its connectedness, although there had been substantial drainage. By 21 March S_W was at the threshold value and the number of cells with $S_N < 1$ in the central portion of the watershed had diminished. Subsequent input events resulted in cells with $S_N > 1$ throughout the watershed (e.g. 12 May). During this time diurnal streamflow peaks were evident in the late afternoon (5 to 6 PM), near the time of peak melt, indicating that water was transferred very rapidly to the channel at this time. As in WY2001, increased evaporative demand and loss of snow cover by mid-May resulted in a rapid drying of the soil and streamflow diminution.

Streamflow amount. A straightforward extension of the conceptual model to estimating the amount of streamflow is that all water passing through the root zone (TF_W) eventually passes over the watershed outlet weir and is counted as streamflow. In an environment such as RME, with very low summer flows, it might be expected that this would be observed, at least approximately, on an annual basis. It is clear, however (Figure 10), that the total TF_W for WY2001 (375 mm) is considerably greater than the streamflow for that time period (289 mm). The 'missing' TF may have left the watershed by deep percolation under or around the weir, been transpired 'downslope' of TF generation, been retained in storage below the root zone, or simply be a result of model error. Whatever the explanation, it does not apply equally to WY2003, because total TF_W and streamflow were practically identical that year ($TF_W = 411$ mm, streamflow = 402 mm). At this point, it appears that further study is required to account for that 'missing' TF.

DISCUSSION

The data presented above indicate that, at RME, streamflow generation is dependent on satiation of soil field capacity over a sufficiently connected spatial domain to generate and transmit TF to the stream channel. Rapid streamflow response is further dependent on maintenance of this wetness condition, which can be described in terms of a threshold watershed storage value, $S_{FC,W}$. These findings have important implications for water management model design but only to the extent that they apply to other watersheds.

We noted previously that threshold-type behaviour has been well documented (Western *et al.*, 2003; Buttle, 2004; Laudon *et al.*, 2004; Tromp-van Meerveld and McDonnell, 2006). However, it may be difficult to quantify a threshold input amount, if one in fact exists, in very humid watersheds that lack a pronounced dry season or have relatively high, variable water tables because soils may rarely if ever dry to S_{PEL} and no consistent zero point can be defined. Western and Grayson (2000) for example, noted that it was very valuable to have a period of extreme dry conditions during their classical study of soil moisture thresholds and connectivity in Australia. On the other hand, Atkinson *et al.* (2002) found that, while soil water storage exerts a dominant control on streamflow for a variety of watersheds in New Zealand, accurate estimation of $S_{FC,W}$ is more critical in relatively dry watersheds, which are more sensitive to that value. In addition, there are many areas where soils may never become satiated. We have noted that, at other locations within the RCEW, a decade may pass before the wet season wetting front passes below 60 cm (Seyfried *et al.*, 2005). Other runoff mechanisms generate streamflow in those environments.

It does appear that stored soil water is a critical element in streamflow generation where overland flow does not generate runoff. The generally observed preponderance of 'old' water in storm flow (Kirchner, 2006; McDonnell *et al.*, 2007) is consistent with the large amount of residual water common in soils (averaging about 160 mm in the RME), combined with the progressive satiation of the soil profile. During periods of rapid flow through the soil profile, even with bypassing, there is a great deal of

DOI: 10.1002/hyp

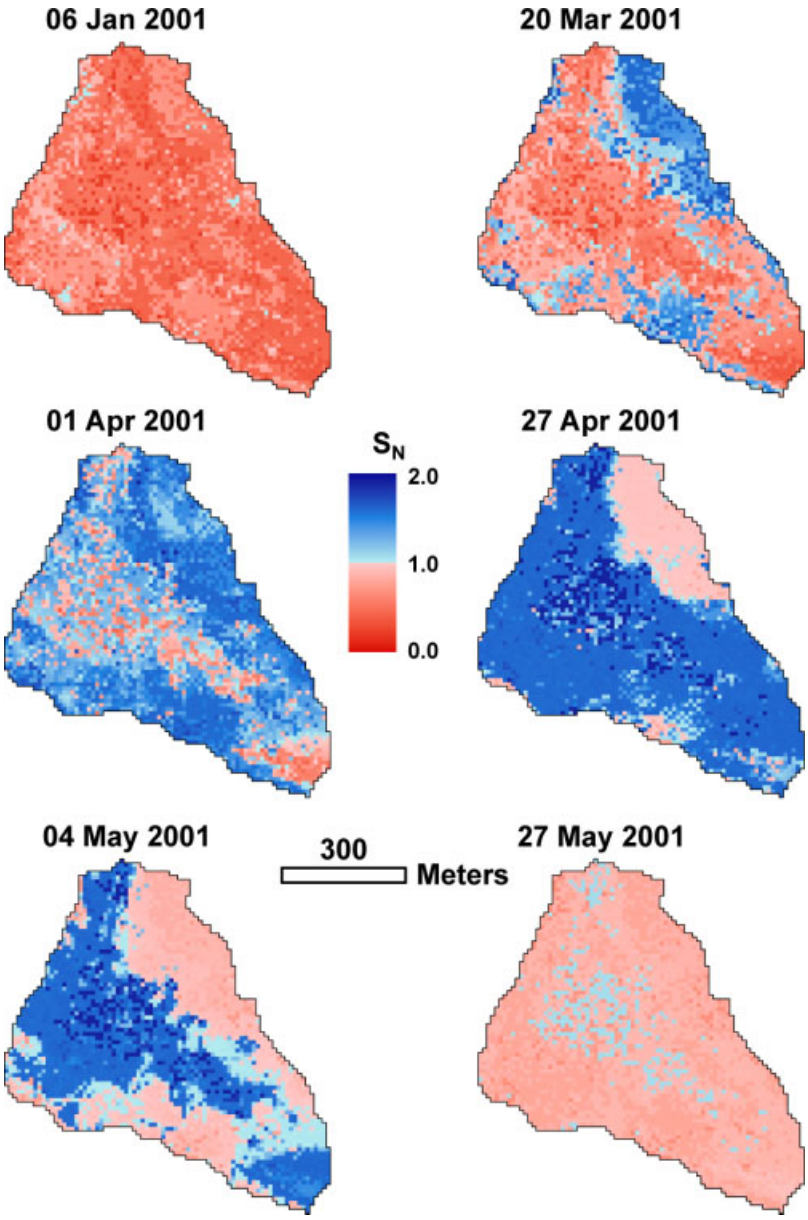

Figure 11. Spatially distributed S_N across the RME watershed for six dates in WY2001. Cells at or above field capacity are represented by S_N values greater than 1.0 and indicate areas that rapidly transmit water through the soil profile

mixing with and displacement of matrix water (Seyfried and Rao, 1987). This 'old' soil water would also likely have different chemical properties from the old aquifer water supplying baseflow in many watersheds, which is another commonly observed chemical trait of streamflow response (Kirchner, 2006). It appears that the critical storage at RME is within the root zone and that, although the water table is probably much deeper, the intervening vadose zone has little porosity and so contributes little to storage. This is clearly not a universal condition, but probably a reasonable assumption in mountainous terrain.

Returning to the snowmelt application, it is significant that the climatic conditions of the mountainous western USA tend to favour the use of soil water storage for estimating streamflow initiation, cessation, and, potentially amount. These are (1) a significant period in which evaporative demand substantially exceeds water supply, soils dry out and stream flows are consistently low, which provides a low point from which to account for added water; (2) low evaporative demand when water accumulates so that changes in soil water are due to infiltration and drainage; (3) storage values continuously at or near $S_{FC,W}$ during snowmelt, so that very rapid streamflow response may be expected; and (4) rapid soil drying and loss of connectivity after snowmelt so that the watershed becomes unresponsive to water inputs.

We have not addressed the critical issue of parameterization of soil water storage, which is beyond the scope of this work. Note, however, recent work that points to the potential of using sparse soil water data to estimate watershed-scale conditions. McNamara *et al*. (2005) described soil water 'states' of consistent, predictable soil water status that are temporally persistent. In addition,

DOI: 10.1002/hyp

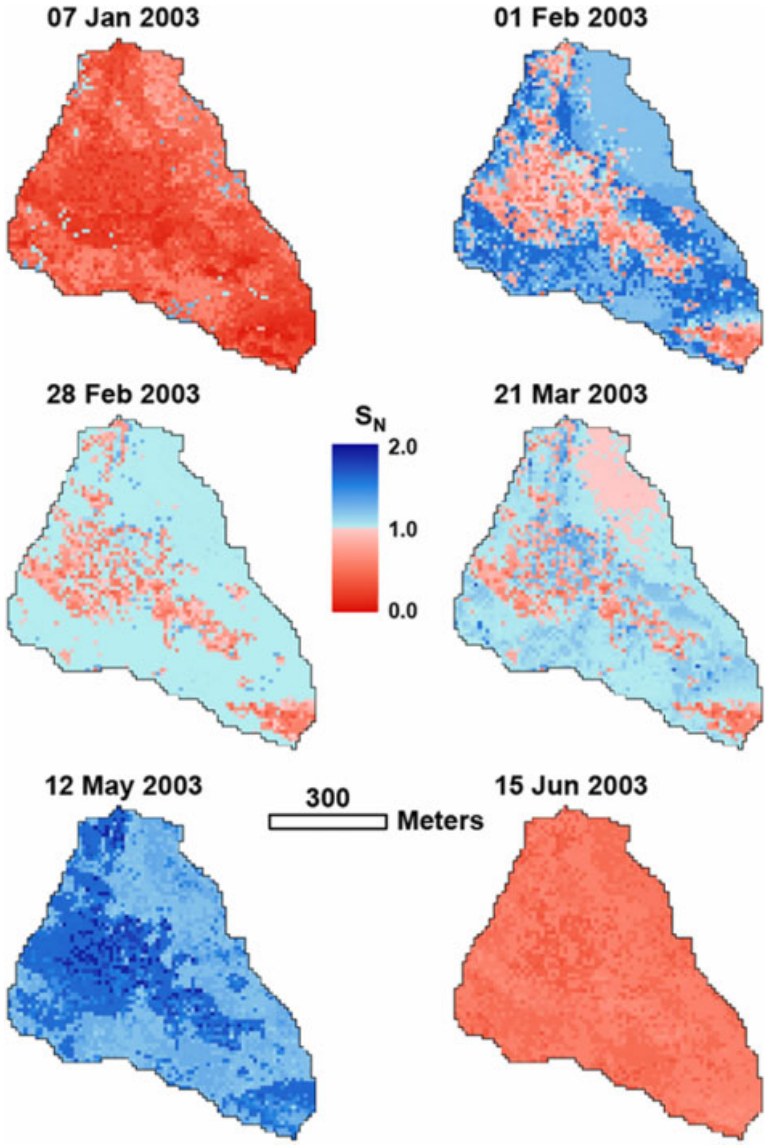

Figure 12. Spatially distributed S_N across the RME watershed for six dates in WY2003. Cells at or above field capacity are represented by S_N values greater than 1.0 and indicate areas that rapidly transmit water through the soil profile

Grant *et al*. (2004) have shown how temporal stability of soil water content widely observed in rainfall dominated systems (Grayson and Western, 1998; Jacobs *et al*., 2004), is also pronounced at RME. However, we must point out that a spatially distributed snowmelt model is critical if we are to take advantage of soil effects on streamflow generation from snowmelt. We suspect that the specialized nature of these models has inhibited the incorporation of soils effects in snowmelt models to date.

REFERENCES

Addiscott TM. 1993. Simulation modeling and soil behaviour. *Geoderma* **60**: 15–40.

Anderson S, Dietrich WE, Montgomery DR, Torres R, Conrad ME, Loague K. 1997. Subsurface flow paths in a steep, unchanneled catchment. *Water Resources Research* **33**(12): 2637–2653.

Atkinson SE, Woods RA, Sivapalan M. 2002. Climate and landscape controls on water balance model complexity over changing timescales. *Water Resources Research* **38**(12): 1314, DOI:10·1029/2002WR001487.

Bales RC, Molotch NP, Painter TP, Dettinger MD, Rice and Dozier J. 2006. Mountain hydrology of the western United Sates. *Water Resources Research* **42**: W08432, DOI:10·1029/2005WR4387.

Barnett TP, Pierce DW, Hidalgo HG, Bonfils C, Santer BD, Das T, Bala G, Wood AW, Nozawa T, Mirin AA, Cayan DR, Dettinger MD. 2008. Human-induced changes in the hydrology of the western United States. *Science* **319**: 1080–1083.

Bazemore DE, Eshleman KN, Hollenbeck KJ. 1994. The role of soil water in stormflow generation in a forested headwater catchment—synthesis of natural tracer and hydrometric evidence. *Journal of Hydrology* **162**: 47–75.

Buttle JM, Dillon PJ, Eerkes GR. 2004. Hydrologic coupling of slopes, riparian zones and streams: an example from the Canadian Shield. *Journal of Hydrology* **287**: 161–177.

Collins R, Jenkins A, Harrow M. 2000. The contribution of old and new water to a storm hydrograph determined by tracer addition to a whole catchment. *Hydrological Processes* **14**: 701–711.

Evans SP, Mayr TR, Hollis JM, Brown CD. 1999. SWBCM: a soil water balance capacity model for environmental applications in the UK. *Ecological Modelling* **121**: 17–49.

Flerchinger GN, Cooley KR, Ralston DR. 1992. Groundwater response to snowmelt in a mountainous watershed. *Journal of Hydrology* **133**: 293–311.

Flerchinger GN, Cooley KR. 2000. A ten-year water balance of a mountainous semi-arid watershed. *Journal of Hydrology* **237**: 86–99.

Gardner WR, Kirkham D. 1952. Determination of soil moisture by neutron scattering. *Soil Science* **73**: 392–401.

Grant L. 2005. *Distribution of soil water dynamics in a small mountain catchment.* MS thesis, Boise State University, Boise, Idaho.

Grant L, Seyfried M, McNamara J. 2004. Spatial variation and temporal stability of soil water in a snow-dominated, mountain catchment. *Hydrological Processes* **18**: 3493–3511.

Grayson RB, Western AW. 1998. Towards aerial estimation of soil water content from point measurements: Time and space stability of mean response. *Journal of Hydrology* **207**(1–2): 68–82.

Hanks RJ. 1974. Model for predicting plant yield as influenced by water use. *Agronomy Journal* **66**: 660–665.

Hanson CL. 2001. Long-term precipitation database, Reynolds Creek Experimental Watershed, Idaho, United States. *Water Resources Research.* **37**(11): 2831–2834.

Hanson CL, Johnson GL. 1993. Spatial and temporal precipitation characteristics in southwestern Idaho. Management of irrigation and drainage systems: Integrated perspectives. In *Proceedings of the 1993 National Conference on Irrigation and Drainage Engineering*. Park City, Utah, Allen R (ed). American Society of Civil Engineers: New York; 394–400.

Hanson CL, Marks DG, VanVactor SS. 2001. Long Term Climate Database, Reynolds Creek Experimental Watershed, Idaho, United States. *Water Resources Research*. **37**(11): 2839–2841.

Hignett C, Evett SR. 2002. Neutron thermalization. In *Methods of Soil Analysis, Part 4, Physical Methods*, Dane JH, Topp GC (eds). *Soil Science Society of America Book Series* 5: Madison: WI; 501–521.

Hillel D. 1980. *Applications of Soil Physics*. Academic Press: New York.

Iwata Y, Hayashi M, Hirota T. 2008. Comparison of snowmelt infiltration under different soil-freezing conditions influenced by snow cover. *Vadose Zone Journal* **7**: 79–86. DOI:10·2136/vzj2007·0089.

Jackson RB, Canadell J, Ehleringer JR, Mooney HA, Sala OE, Schulze ED. 1996. A global analysis of root distributions for terrestrial biomes. *Oecologia* **108**: 389–411.

Jacobs JM, Mohanty BP, Hsu E, Miller D. 2004. SMEX02: Field scale variability, time stability and similarity of soil moisture. *Remote Sensing of Environment* **92**: 436–446.

James AL, Roulet NT. 2007. Investigating hydrologic connectivity and its association with threshold change in runoff response in a temperate forested watershed. *Hydrological Processes* **21**: 3391–3408.

Kirchner JW. 2006. Getting the right answers for the right reasons: Linking measurements, analysis, and models to advance the science of hydrology. *Water Resources Research* **42**: W03S04, DOI:10·1029/2005WR004363.

Ladson AR, Lander JR, Western AW, Grayson RB, Zhang L. 2006. Estimating extractable soil moisture content for Australian soils from field measurements. *Australian Journal of Soil Research* **44**: 531–541.

Laudon H, Seibert J, Kohler S, Bishop K. 2004. Hydrological flow paths during snowmelt: Congruence between hydrometric measurements and oxygen 18 in meltwater, soil water, and runoff. *Water Resources Research* **40**: W03102, DOI:10·1029/2003WR002455.

Lindström G, Bishop K, Löfvenius MO. 2002. Soil frost and runoff at Svartberget, northern Sweden—measurements and model analysis. *Hydrological Processes* **16**: 3379–3392.

Marks D. 2001. Introduction to special section: Reynolds Creek Experimental Watershed. *Water Resources Research* **37**: 2817.

Marks D, Domingo J, Frew J. 1999a. Software tools for hydroclimatic modeling and analysis: Image Processing Workbench, ARS-USGA Version2. Northwest Watershed Research Center, USDA Agricultural Research Service, Boise, Idaho. ARS Technical Bulletin 99-1. http://www.nrcs.usda.gov.

Marks D, Domingo J, Susong D, Link T, Garen D. 1999b. A spatially distributed energy balance snowmelt model for application in mountain basins. *Hydrological Processes* **13**: 1935–1959.

Marks D, Winstal A, Seyfried M. 2002. Simulation of terrain and forest shelter effects on patterns of snow deposition, snowmelt and runoff over a semi-arid mountain catchment. *Hydrological Processes* **16**: 3605–3626.

McDonnell JJ, Sivapalan M, Vache K, Dunn S, Grant G, Haggerty R, Hinz D, Hooper R, Kirchner J, Roderick ML, Selker J, Weiler M. 2007. Moving beyond heterogeneity and process complexity: a new vision for watershed hydrology. *Water Resource Research* **43**: W07301, DOI:10·1029/2006WR005467.

McNamara JP, Chandler D, Seyfried M, Achet S. 2005. Soil moisture states, lateral flow, and streamflow generation in a semi-arid, snowmelt-driven catchment. *Hydrological Processes* **19**: 4023–4038.

Mulla D, Addiscott TM. 1999. Validation approaches for field-, basin-, and regional-scale water quality models. In *Assessment of Non-Point Source Pollution in the Vadose Zone*, Corwin DL, Loague K, Ellsworth TR (eds). *Geophysical Monograph* 108, American Geophysical Union: Washington, DC.

Nayak A, Marks D, Chandler DG, Seyfried M. submitted. Long-term snow, climate, and streamflow from the Reynolds Creek Experimental Watershed. *Water Resources Research*.

Or D, Wraith JM. 2002. Soil water content and water potential relationships. In *Soil Physics Companion*, Warrick AW (ed). CRC Press: New York; 49–84.

Peters NE, Freer J, Aulenbach BT. 2003. Hydrological dynamics of the Panola Mountain Research Watershed, Georgia. *Ground Water* **41**: 973–988.

Pierson Jr FB, Slaughter CW, Cram ZK. 2001. Long-term stream discharge and suspended sediment database Reynolds Creek Experimental watershed Idaho USA. *Water Resources Research*. **37**(11): 2857–2861.

Pockman WT, Sperry JS. 2000. Vulnerability to cavitation and the distribution of Sonoran Desert vegetation. *American Journal of Botany* **87**: 1287–1299.

Priestly CHB, Taylor RJ. 1972. On the assessment of surface heat flux and evaporation using large scale parameters. *Monthly Weather Review* **100**: 81–92.

Ratliff LF, Ritchie JT, Cassel DK. 1983. Field-measured limits of soil water availability as related to laboratory-measured properties. *Soil Science Society of America Journal* **47**: 770–775.

Ritchie JT. 1981. Water dynamics in the soil-plant-atmosphere system. *Plant and Soil* **58**: 81–96.

Rose CW. 1984. Modelling evapotranspiration: an approach to heterogeneous communities. *Agricultural Water Management* **8**: 203–210.

Saxton KE, Rawls WJ. 2006. Soil water characteristic estimates by texture and organic matter for hydrologic solutions. *Soil Science Society of America Journal* **70**: 1569–1578.

Schneiderman EM, Steenhuis TS, Thongs DJ, Easton ZM, Zion MS, Neal AL, Mendoza GF, Walter MT. 2007. Incorporation variable source area hydrology into a curve-number-based watershed model. *Hydrological Processes* **21**: 3420–3430.

Seyfried MS. 2003. Incorporation of remote sensing data in an upscaled soil water model. In *Scaling Methods in Soil Physics*, Pachepsky Y, Radcliffe DE, Selim HS (eds). CRC Press: New York; 309–346.

Seyfried MS, Rao PSC. 1987. Solute transport in undisturbed columns of an aggregated tropical soil: preferential flow effects. *Soil Science Society of America Journal* **51**: 1434–1444.

Seyfried MS, Rao PSC. 1991. Nutrient leaching loss from two contrasting cropping systems in the humid tropics. *Tropical Agriculture* **68**: 9–18.

Seyfried MS, Wilcox BP. 1995. Scale and the nature of spatial variability: field examples having implications for hydrologic modeling. *Water Resources Research* **31**: 173–184.

Seyfried MS, Hanson CL, Murdock MD, Van Vactor S. 2001a. Long-term lysimeter Database, Reynolds Creek Experimental Watershed, Idaho, USA. *Water Resources Research* **37**: 2853–2856.

Seyfried MS, Harris R, Marks D, Jacob B. 2001b. Geographic database, Reynolds Creek Experimental Watershed, Idaho, United States. *Water Resources Research* **37**(11): 2825–2830.

Seyfried MS, Murdock MD, Hanson CL, Flerchinger GN, Van Vactor SS. 2001c. Long-term soil water content database, Reynolds Creek Experimental Watershed, Idaho, United States. *Water Resources Research* **37**(11): 2847–2852.

Seyfried MS, Schwinning S, Walvoord MA, Pockman WT, Newman BD, Jackson RB, Phillips FM. 2005. Ecohydrological control of deep drainage in arid and semiarid regions. *Ecology* **86**: 277–287.

Shuttleworth WJ. 1993. Evaporation. In *Handbook of Hydrology*, Maidment DR (ed). McGraw Hill: New York; 4·1–4·53.

Steenhuis TS, Winchell M, Rossing J, Zollweg WA, Walter MF. 1995. SCS runoff equation revisited for variable-source runoff areas. *American Society of Civil Engineers, Journal of Irrigation and Drainage Engineering* **121**: 234–238.

Tromp-van Meerveld HJ, McDonnell JJ. 2006. Threshold relations in subsurface stormflow: 2. The fill and spill hypothesis. *Water Resources Research* **42**: W02411, DOI:10·1029/2004WR003800.

Western A, Grayson R. 2000. Soil moisture and runoff processes at Tarrawarra. In *Spatial Patterns in Catchment Hydrology: Observations and Modelling*, Grayson R, Bloschl G (eds). Cambridge University Press: Cambridge; 209–246.

Western AW, Grayson RB, Bloschl G, Wilson DJ. 2003. Spatial variability of soil moisture and its implications for scaling. In *Scaling Methods in Soil Physics*, Pachepsky Y, Radcliffe DE, Selim HS (eds). CRC Press: New York; 119–138.

Whitaker AC, Sugiyama H. 2005. Seasonal snowpack dynamics and runoff in a cool temperature forest: lysimeter experiment in Niigata, Japan. *Hydrological Processes* **19**: 4179–4200.

Wierenga PJ, Hills RG, Hudson DB. 1991. The Las Cruces Trench site: characterization, experimental results, and one-dimensional flow predictions. *Water Resources Research* **27**: 2695–2705.

Wilcox BP, Newman BD, Brandes D, Davenport DW, Reid K. 1997. Runoff from a semiarid ponderosa pine hillslope in New Mexico. *Water Resources Research* **33**: 2301–2311.

Williams CJ, McNamara JP, Chandler DG. 2008. Controls on the temporal and spatial variability of soil moisture in a mountainous landscape: the signatures of snow and complex terrain. *Hydrology and Earth System Sciences Discussions* **5**: 1927–1966.

Winstral A, Marks D. 2002. Simulating wind fields and snow redistribution using terrain-based parameters to model snow accumulation and melt over a mountain catchment. *Hydrological Processes* **16**: 3585–3603. DOI:10·1002/hyp.1238.

Winstral A, Marks D, Gurney R. 2008. An efficient method for distributing wind speeds over heterogeneous terrain. *Hydrological Processes* (in press).

Zhang T. 2005. Influence of the seasonal snow cover on the ground thermal regime: an overview. *Reviews of Geophysics* **43**: RG4002, DOI:10·1029/2004RG000157.